

## 論文

## Micromechanical 시험법과 음향방출을 이용한 Implant용 Bioabsorbable 복합재료의 미세파괴 분해메커니즘과 계면물성

박종만<sup>\*\*</sup>, 김대식<sup>\*</sup>

### Microfailure Degradation Mechanisms and Interfacial Properties of Bioabsorbable Composites for Implant Materials using Micromechanical Technique and Acoustic Emission

J. M. Park<sup>\*\*</sup>, D. S. Kim<sup>\*</sup>

#### ABSTRACT

Interfacial properties and microfailure degradation mechanisms of the bioabsorbable composites for implant materials were investigated using micromechanical technique and nondestructive acoustic emission (AE). As hydrolysis time increased, the tensile strength, the modulus and the elongation of poly(ester-amide) (PEA) and bioactive glass fibers decreased, whereas those of chitosan fiber almost did not change. Interfacial shear strength (IFSS) between bioactive glass fiber and poly-L-lactide (PLLA) was much higher than PEA or chitosan fiber/PLLA systems using dual matrix composite (DMC) specimen. The decreasing rate of IFSS was the fastest in bioactive glass fiber/PLLA composites whereas that of chitosan fiber/PLLA composites was the slowest. AE amplitude and AE energy of PEA fiber decreased gradually, and their distributions became narrower than those in the initial state with hydrolysis time. In case of bioactive glass fiber, AE amplitude and AE energy in tensile failure were much higher than in compression. In addition, AE parameters at the initial state were much higher than those after degradation under both tensile and compressive tests. In this work, interfacial properties and microfailure degradation mechanisms can be important factors to control bioabsorbable composite performance.

#### 초 록

Implant용 bioabsorbable 복합재료의 계면물성과 미세파괴분해 메커니즘을 micromechanical 시험법과 음향방출을 이용하여 평가하였다. Poly(ester-amide)와 bioactive 유리섬유의 인장 강도와 탄성률 그리고 연신율은 분해시간에 따라 점차적으로 감소하는 경향을 보인 반면, chitosan 섬유는 분해시간 내에서 거의 변화가 없었다. Dual matrix composite 시험법을 이용하여 측정된 bioactive 유리섬유와 poly(L-lactide) 사이의 계면전단강도는 chitosan이나 poly(ester-amide) 섬유의 경우 보다 큰 값을 보였다. 그리고 계면전단강도 감소는 bioactive 유리섬유 강화 poly(L-lactide) 복합재료에서 가장 빨랐으며, chitosan 섬유의 경우가 상대적으로 가장 느린 경향을 보였다. Poly(ester-amide) 섬유의 분해시간에 따른 음향방출

<sup>\*\*</sup> 경상대학교 응용화학공학부/고분자공학전공, 항공기부품기술연구센터, 교신저자 (E-mail:jmpark@nongae.gsnu.ac.kr)

<sup>\*</sup> 경상대학교 응용화학공학부/고분자공학전공, 대학원

진폭과 에너지는 점차로 감소하였고, 음향방출 진폭의 분포 역시 점차 좁아짐을 보여주었다. Bioactive 유리섬유에서 인장과단에 의한 음향방출 진폭과 에너지는 압축과단의 경우 보다 크게 나타났으며, 또한, 인장 및 압축시험 모두에서 초기상태가 분해 후 보다 더 큰 값을 보였다. 본 연구에서 평가한 계면물성과 미세파괴분해 메카니즘은 생흡수성 복합재료의 성능을 조절할 수 있는 중요한 요소가 될 것이다.

## 1. INTRODUCTION

Bioabsorbable bone fixation, screw and rods can offer the major advantages over conventional metallic implants as follows: the need for removal surgery is obviated [1] and the financial savings [2]. In addition, the degradation byproducts are biocompatible in contrast to harmful metallic ions and the elastic modulus is closer to that of bone, which could minimize the stress concentration near the edge of the implants [3]. Because the currently available absorbable polymer materials in alone have the insufficient modulus and the strength for certain demanding implant applications, many works on bioabsorbable fiber reinforced composite materials has been currently investigated [4]. Bioabsorbable fiber reinforced composites can provide higher strength and elastic modulus as well as better fatigue properties. It is also important to know each microfailure mechanisms of either bioabsorbable fiber or matrix with hydrolysis, respectively.

Chu *et al.* [5] measured the decreasing IFSS of calcium phosphate (CaP) or chitin fibers reinforced PLLA composites with hydrolysis time by microdroplet and single fiber composite (SFC) tests, and also measured the interfacial gap width between bioabsorbable fiber and matrix *via* laser scanning confocal microscopy (LCSM). Daniels [6] reported that the initial mechanical properties and degradation kinetics measured for the design of absorbable fracture fixation devices. They evaluated the changes of mechanical properties of self-reinforced poly(glycolide) (SR-PGA) and poly(ortho-ester) (POE) fixation pins implanted directly into bone of animal. Pennings *et al.* [7] predicted the degree of degradation by measuring molecular weight of PLLA and poly(ethylene-oxide) blends. However, there are few studies correlated with interfacial properties and microfailure degradation modes of bioabsorbable composites using micromechanical test and nondestructive evaluation together.

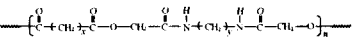
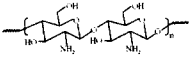
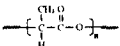
The SFC test method [8], originally proposed by Kelly and Tyson [9] for fiber/metal composite, can provide abundant statistical information, such as microfailure modes of

reinforcing fiber and interface between fiber and matrix, and IFSS, using only a few specimens. In SFC test the failure elongation of the matrix should be several times larger than the failure elongation of the fiber to cause a saturated fragmentation state. This conventional SFC method cannot be adequate for less brittle fiber/brittle matrix composite system. DMC test [10] is basically modified from the SFC test. Park *et al.* [11] studied interfacial properties and microfailure mechanisms of DMC for single glass fiber/brittle unsaturated polyester/ductile epoxy using micromechanical technique and AE.

Recently, the single fiber Broutman test [12] was used to know interfacial properties and microfailure mechanism by subjecting to apply compressive tensile load in a single necked specimen. Under compressive load, the interfacial debonding and buckling behavior were investigated with an aid of AE. Marom *et al.* [13] studied the compressive fragmentation phenomenon using microcomposites to evaluate thermal stresses, single fiber compressive strength and their IFSS. AE is well known as one of the important nondestructive (NDT) testing methods [14]. AE can monitor the fracture behavior of a composite structure, and characterize AE parameters to understand the type of fracture sources and their progressing. When the tensile loading is applied to a composite material, many AE signals may occur from fiber fracture, matrix cracking, and interfacial failure. Generally, the AE energy released by fiber fracture should be greater than that associated by matrix cracking or debonding [15].

In this work, the degradation for bioabsorbable fibers was investigated *via* optical observation of fiber surface morphology, measurement of changed fiber diameter and tensile strength. IFSS of bioabsorbable fibers reinforced PLLA composites was also measured as a function of hydrolysis time by DMC test. Fiber fracture signals were detected by AE under either tensile fragmentation or compressive Broutman tests and then correlated with their microfailure modes.

**Table 1** Chemical structure of two bioabsorbable fibers and PLLA matrix.

Fiber	Chemical Structure
PEA <sup>1)</sup>	
Chitosan <sup>2)</sup>	
PLLA <sup>3)</sup>	

1) 3M Co. 2) RC Bio-Chemical Co., Korea  
3) Sigma-Aldrich Co.

## 2. EXPERIMENTAL

### 2.1 Materials

PEA fiber (3M Co.) commercially available for surgical suture and chitosan fiber (RC-Biochemical Co., Korea) were used and their average diameters were 30 and 15  $\mu\text{m}$ . Measured tensile strength values for PEA and chitosan fibers were about 206 and 187 MPa, whereas Youngs moduli of two fibers were 4 and 16 GPa, respectively. Chemical structures of the bioabsorbable fibers and matrix were shown in Table 1. Chemical structure of the chitosan is similar to that of chitin or cellulose. The structures of chitin and cellulose are composed of acetyl and hydroxyl groups instead of amine group of chitosan. Bioactive glass fiber (Institute of biomaterials, Finland) as ceramic-type bioabsorbable fiber was used to compare to bioabsorbable polymeric fiber. Average diameter was 40  $\mu\text{m}$  and their tensile strength and modulus were about 660 MPa and 67 GPa, respectively. Bioactive glass fiber has atomic compositions of 52.0% in Si, 19.4% in Ca, 15.3% in K, 7.7% in Na and 5.6% in Mg etc.

PLLA (Sigma-Aldrich Co.) was used as matrix and the range of molecular weight was from 85,000 to 160,000. PLLA is semicrystalline and bioabsorbable thermoplastic polymer. The melting temperature,  $T_m$  of PLLA is about 180  $^{\circ}\text{C}$  and the glass transition temperature,  $T_g$  is about 57  $^{\circ}\text{C}$ . Epoxy resin (YD-128, Kukdo Chemical Co., Korea) was used as a supporting matrix in DMC test and it is based on diglycidylether of bisphenol-A (DGEBA). Polyoxypropylene-diamine (Jeffamine D400 and D2000, Huntsman Petrochemical Co.) was used as curing agents. Flexibility of the

specimen was controlled by adjusting the relative ratio of D400 versus D2000 in the curing mixture.

### 2.2 Methodologies

#### 2.2.1 Measurement of Single-Fiber Tensile Strength Under Hydrolysis

PEA, chitosan and bioactive glass fibers were fixed on the acryl frame using Kapton tape, and they were hydrolyzed in deionized water. In order to accelerate the degradation, temperature was elevated up to 70  $^{\circ}\text{C}$  in a clean oven. The degradation time was ranged as the initial state, 1, 3, 5 and 10 days, respectively. The tensile strength of bioabsorbable fibers with hydrolysis time at various gauge lengths was obtained using about fifty specimens for statistically meaningful value using Weibull distributions.

Average diameter was measured by an optical microscope attached with a calibrated eyes piece. Single fiber was placed in the centerline on the middle of a paper frame, and fixed the fiber using Scotch tape, and then finally glued the fiber by an epoxy adhesive. Universal testing machine (UTM) (LR-10K, Lloyd Instrument Ltd., U.K.) was used to measure the single fiber tensile strength. Used load cell was 10 N with a small capacity and the crosshead speed was 1 mm/minute.

#### 2.2.2 Specimens Preparation

Tensile and compressive tests were applied to investigate the microfailure modes and AE parameters of bioabsorbable fiber with hydrolysis time. Single fiber tensile and compressive specimens were made by bioabsorbable fiber embedded in epoxy matrix in silicone mould. It was precured for 3 days at 25  $^{\circ}\text{C}$  and then 2 hours at 80  $^{\circ}\text{C}$  and finally postcured for 2 hours at 120  $^{\circ}\text{C}$ . Tensile specimens were tested axially by universal testing machine with 10 KN load cell and crosshead speed of 0.5 mm/minute. For comparison, the compressive test was tested with a crosshead speed of 2 mm/minute only for bioactive glass fiber.

DMC test was performed to measure the IFSS between bioabsorbable fiber and matrix. Figure 1 shows a scheme of DMC specimen. Bioabsorbable fibers were coated using PLLA solved in dichlormethane and coating thickness was controlled uniformly as about 80  $\mu\text{m}$ . Hydrolysis temperature was established at 37  $^{\circ}\text{C}$  in the incubator. The degradation

time was ranged as the initial state, 5, 10, 15 and 20 days at evaluating temperature, respectively. Bioabsorbable fiber coated with PLLA was embedded again in epoxy resin and then cured for 3 days at room temperature. Epoxy resin in the DMC specimen was used only as a supporting matrix to perform DMC testing.

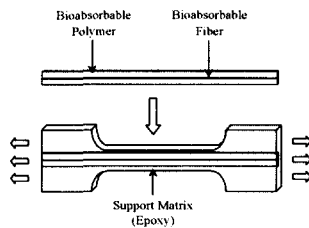


Fig. 1 Scheme of DMC test

The DMC specimen was stressed incrementally during testing and the fiber was fractured into small fragments within the PLLA matrix. As the tensile stress was applied, the fracture process continued until the fracture ceased in the specimen. At this strain an ultimate fragment length attained a critical length,  $L_c$ . Ultimate fragment length within the matrix was measured and the subsequent failure process was observed *via* a polarized-light microscope. Surface topography of bioabsorbable fibers was observed by scanning electron microscope (SEM, Model JSM6400, JOEL Co.) The fibers were coated with gold sputtering for 300 seconds before observation, and working distance in SEM was 18 mm.

### 2.2.3 IFSS Measurement

The IFSS of bioabsorbable fibers/PLLA composites was calculated from both Kelly-Tyson (1) and Drzal equations (2). Based on the force balance in a micromechanical model, Kelly and Tyson [9] showed that IFSS,  $\tau$  is given by

$$\tau = \frac{\sigma_f \cdot d}{2 \cdot L_c} \quad (1)$$

where  $d$  is the fiber diameter,  $\sigma_f$  is the single fiber tensile strength at the critical fragment length  $L_c$ . Drzal *et al.* [16] altered the equation (1) to reflect Weibull statistics to form

$$\tau = \frac{\sigma_f}{2 \cdot \alpha} \cdot \Gamma \left[ 1 - \frac{1}{\beta} \right] \quad (2)$$

where  $\alpha$  and  $\beta$  are the scale and shape parameters in the Weibull distribution for the aspect ratio and  $\Gamma$  is Gamma function.

Fiber strength can be calculated from the extrapolation gauge length using Weibull weakest link rule [20]. The fiber strength,  $\sigma_f$  at the critical fragment length is

$$\sigma_f = \sigma_{f0} \cdot \left( \frac{L_c}{L_0} \right)^{-\frac{1}{\rho}} \quad (3)$$

where  $\sigma_{f0}$  is fiber strength at gauge length,  $L_0$  and  $\rho$  is shape parameter of Weibull distribution for the fiber tensile strength.

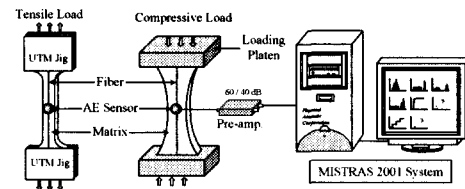


Fig. 2 Scheme of the instrumentation for AE

### 2.2.4 AE Measurement

Figure 2 shows the experimental system of AE test for tensile and compressive tests. Testing specimen was placed on the UTM and AE sensor was attached in the center of the specimen using vacuum grease couplant. AE signals were detected using a miniature sensor (Resonance Type, R15 model by PAC) with peak sensitivity of -64 Ref. V/mbar and resonant frequency at 150 kHz. The sensor output was amplified by either 40 dB or 60 dB at preamplifier and passed through a band-pass filter with a range of 50 kHz to 200 kHz. The threshold level was set as 35 dB. The signal was fed into an AE signal process unit (MISTRAS 2001 System) and AE parameters were analyzed using in-built software. Typical AE parameters such as peak amplitude and energy were investigated in terms of the testing time and the distribution.

**Table 2 Comparison of mechanical properties for bioabsorbable and nonbioabsorbable fibers**

Type	Fiber	Tensile Strength (MPa)	Tensile modulus (GPa)	Elongation (%)
Bioabsorbable	PEA	206 (47) <sup>1)</sup>	4.0 (0.9)	7.8 (1.6)
	Chitosan	187 (54)	16.3 (4.8)	7.4 (2.2)
	Bioactive glass	670 (216)	66.5 (12.5)	1.1 (0.3)
Nonbioabsorbable	Carbon	2666 (707)	221.5 (18.8)	1.4 (0.4)
	Glass	1485 (377)	58.6 (7.6)	2.2 (0.6)

1) Parentheses are standard deviation (SD). \* Gauge length: 20 mm

**Table 3 Mechanical Properties and Weibull distribution parameters of bioabsorbable fibers for various gauge lengths**

Fiber	Gauge length (mm)	$\alpha$ <sup>1)</sup>	$\beta$ <sup>2)</sup>	COV <sup>3)</sup>	Tensile Strength (MPa)	Tensile modulus (GPa)	Elongation (%)
PEA	2	317	3.6	32	285 (92) <sup>4)</sup>	2.1 (1.0)	18.1 (7.7)
	5	270	4.4	25	246 (62)	2.9 (0.9)	10.9 (2.4)
	10	256	3.2	29	228 (67)	3.4 (1.1)	9.5 (1.1)
	20	225	4.7	22	206 (47)	4.0 (0.9)	7.8 (1.6)
	50	198	5.8	17	183 (31)	4.2 (0.5)	7.6 (1.7)
Chitosan	2	315	4.4	24	287 (71)	7.1 (3.0)	21.2 (3.7)
	5	265	3.0	40	236 (95)	7.7 (4.3)	12.0 (2.6)
	10	232	3.1	37	206 (77)	12.1 (3.5)	9.3 (2.6)
	20	206	4.0	29	187 (54)	16.3 (4.8)	7.4 (2.2)
	100	121	4.2	28	110 (30)	18.4 (5.0)	2.8 (0.6)
Bioactive glass	2	776	5.8	14	722 (98)	212.5 (30)	0.7 (0.3)
	20	744	3.6	32	671 (216)	66.5 (12.5)	1.1 (0.3)

1) Scale parameter for fiber tensile strength      2) Shape parameter for fiber tensile strength  
 3) Coefficient of variation (COV) (%) = SD/Mean × 100      4) Parentheses are standard deviation (SD).

### 3. RESULTS AND DISCUSSION

#### 3.1 Mechanical Properties and Degradation Mechanisms of Fibers with Hydrolysis

Table 2 shows the mechanical properties of bioabsorbable and nonbioabsorbable fibers. Tensile strength and modulus of bioabsorbable fibers are normally much lower than those of nonbioabsorbable fibers. Bioabsorbable fiber has special characteristics that are degraded finally by hydrolysis. The tensile strength of most brittle ceramic fibers is known to be strongly dependent upon the gauge length. This is probably due to the surface flaws along the fiber [18]. On the other hand, since polymeric fibers may occur local plastic deformation, it may be relatively less dependent upon the gauge length than ceramic type fiber.

Table 3 shows the mechanical properties and Weibull

distribution parameters of PEA, chitosan and bioactive glass fibers with various gauge lengths. As the gauge length increased, both the tensile strength and the elongation of three bioabsorbable fibers decreased. Diameter of chitosan fiber was much smaller than that of PEA fiber, whereas tensile strength was similar to each other and tensile modulus was much higher. It may be due to the fibril structure of chitosan fiber compared to PEA fiber with monofilament structure. Tensile strength and modulus of bioactive glass fiber were much higher than PEA and chitosan fibers because of ceramic type, whereas the elongation was much lower than other two polymeric fibers. Scale parameters, indicating the scale of mean value, of PEA and chitosan fibers decreased gradually with increasing gauge length, whereas shape parameter did not show significant difference in both cases. Shape parameter means statistical data scattering and the degree of half width in Weibull distribution curve for fiber

Table 4 Mechanical Properties and Weibull distribution parameters of PEA, chitosan and bioactive glass fibers with hydrolysis time

Fiber	Hydrolysis Time (day)	$\alpha$ <sup>1)</sup>	$\beta$ <sup>2)</sup>	COV <sup>3)</sup>	Tensile Strength (MPa)	Tensile modulus (GPa)	Elongation (%)
PEA	0	225	4.7	22	206 (46) <sup>4)</sup>	4.0 (0.9)	7.8 (1.6)
	1	161	2.9	38	143 (55)	2.9 (1.5)	7.6 (1.3)
	3	114	3.5	27	102 (33)	2.5 (0.9)	7.2 (1.0)
	5	89	3.2	35	80 (28)	2.7 (0.9)	4.6 (1.5)
	10	56	3.3	35	51 (18)	2.9 (0.9)	3.5 (1.1)
Chitosan	0	187	4.0	29	187 (54)	16.3 (4.8)	7.2 (2.2)
	1	182	4.5	24	182 (45)	14.5 (4.9)	6.9 (1.8)
	3	222	4.5	18	222 (41)	13.7 (3.3)	6.2 (2.2)
	5	190	5.8	18	190 (34)	13.6 (3.2)	6.0 (2.2)
	10	210	6.9	14	210 (30)	13.2 (2.1)	6.1 (1.8)
Bioactive glass	0	744	3.6	32	671 (216)	66.5 (12.5)	1.1 (0.3)
	1	583	4.5	24	557 (131)	55.6 (11.4)	0.9 (0.2)
	3	301	3.8	34	271 (92)	45.1 (14.0)	0.8 (0.1)

1) Scale parameter for fiber tensile strength

2) Shape parameter for fiber tensile strength

3) Coefficient of variation (COV) (%) = SD/Mean × 100

4) Parentheses are standard deviation (SD).

tensile strength. As shape parameter becomes smaller, Weibull distribution curve appears relatively broader.

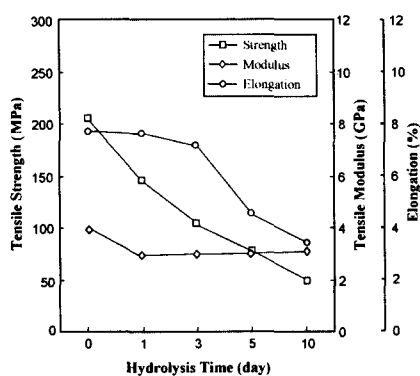


Fig. 3 Mechanical properties for PEA fiber with hydrolysis time

The mechanical properties and Weibull distribution parameters of PEA, chitosan and bioactive glass fibers as a function of hydrolysis time at 70°C are shown in Table 4. Figures 3, 4 and 5 show the plots for mechanical properties of 3 bioabsorbable fibers. The tensile strength, the modulus and the elongation of PEA fiber decreased continuously. At 3 and 10 days, the tensile strength of PEA fiber became a half and a quarter compared to the initial state, respectively. On the other hand, the elongation of PEA fiber decreased steeply. It might be due to the brittleness resulted from deteriorated

molecular weight with hydrolysis time. The tensile properties of chitosan fiber changed little within the testing time. For bioactive glass fiber, the mechanical properties decreased steeply because degradation rate was fast. At 3 days the tensile strength of bioactive glass fiber became one third compared to the initial state.

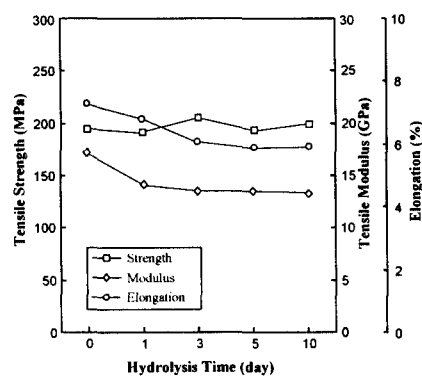
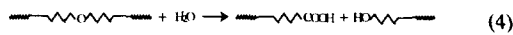


Fig. 4 Mechanical properties for chitosan fiber with hydrolysis time

The hydrolytic degradation may start to occur in the amorphous region and then progressed toward the crystalline domains. This hydrolysis mechanism results in the changes of several property parameters such as molecular weight and strength, mass, diameter, degree of crystallinity and surface

morphology etc [19]. Figure 6 shows the scheme of possible hydrolysis mechanisms for bioabsorbable fiber. It might induce propagation of microcracks and decrease diameter gradually. A hydrolysis of bioabsorbable fiber may create more polar hydrophilic groups such as hydroxyl and carboxyl on the fiber surface [19]. The simplified hydrolysis reaction on bioabsorbable fiber surface is generally as



As the hydrolysis time increased, bioabsorbable polymeric chain may be degraded to become low molecules, and finally they are dissolved into water.

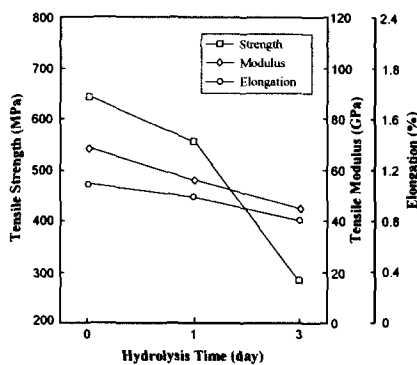


Fig. 5 Mechanical properties for bioactive glass fiber with hydrolysis time

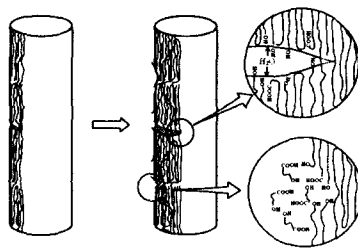


Fig. 6 Possible hydrolysis mechanisms of bioabsorbable fibers

Figure 7 show SEM photographs of PEA fiber after sufficient hydrolysis time elapsed. Microcracks were propagated into the fiber along cross-sectional plane. Hydrolytic resistance is known to be rather weak in cross-sectional direction of fiber because amorphous regions are less dense than the crystalline domain [19]. Figure 8

shows the changes of diameter for PEA, chitosan and bioactive glass fibers with hydrolysis time at elevated 70°C. PEA fiber decreased slightly and chitosan fiber changed little, whereas the diameter of bioactive glass fiber decreased rapidly. It could be confirmed that the degradation rate of bioabsorbable fiber with higher hydrophilicity was fast. In case of the bioactive glass fiber treated properly by hydrophobic material such as plasma treated with methane gas, the stability for hydrolytic degradation might be improved.

### 3.2 Comparison of IFSS with Hydrolysis Time

DMC test was applied to investigate the interfacial properties of fiber reinforced brittle matrix composites in our previous work [11]. This DMC method was also adopted for ductile bioabsorbable matrix such as PLLA and PGA. DMC specimen is composed of a single bioabsorbable fiber, and rectangular film-shaped PLLA coating layer as an inner matrix, plus ductile epoxy matrix as a supporting outer matrix. The specimen is subjected to tensile load and resulted in many fragments of the embedded fiber, whereas the failure of coating layer does not appear because their elongation is close to those of supporting matrix. Results obtained from DMC test can be considered to be same as the conventional SFC test, by assuming the perfect bonding of the interface between PLLA inner matrix and epoxy outer matrix. DMC specimen can have significant advantages, such as cost saving of expensive PLLA matrix as well as testing time.

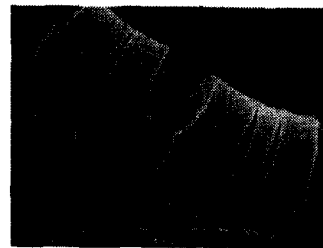


Fig. 7 SEM photograph of PEA fiber after degradation

Figure 9 shows the changes of IFSS for PEA, chitosan or bioactive glass fibers/PLLA composites with hydrolysis time in DMC test. Especially, initial IFSS between bioactive glass fiber and PLLA was significantly higher than that of other

Table 5 IFSS of bioabsorbable fibers/PLLA composites with hydrolysis time

Fiber	Hydrolysis Time (day)	Ave. Fragments Length ( $\mu\text{m}$ )	$\alpha$ <sup>1)</sup>	$\beta$ <sup>2)</sup>	IFSS (MPa)	
					Kelly-Tyson	Drzal
0	PEA	356 (22) <sup>3)</sup>	12.2 (1.8)	4.3 (0.3)	14.3 (2.8)	15.5 (3.2)
	Chitosan	112 (21)	8.2 (1.5)	3.6 (0.3)	19.5 (2.4)	21.3 (3.1)
	Bioactive glass	463 (28)	13.2 (2.3)	3.8 (1.4)	31.2 (4.2)	35.1 (5.8)
5	PEA	340 (20)	10.6 (2.0)	4.1 (0.2)	15.1 (3.4)	16.7 (4.0)
	Chitosan	104 (22)	7.7 (1.5)	3.3 (0.3)	20.8 (2.1)	22.4 (3.5)
	Bioactive glass	663 (37)	18.8 (3.5)	3.5 (1.3)	22.6 (2.1)	28.2 (3.5)
10	PEA	333 (18)	10.9 (1.7)	3.6 (0.4)	15.0 (3.1)	16.1 (3.6)
	Chitosan	98 (23)	7.5 (1.7)	4.1 (0.3)	21.1 (2.2)	22.6 (3.8)
	Bioactive glass	989 (43)	17.4 (4.6)	4.2 (1.5)	14.6 (3.5)	17.8 (4.2)
15	PEA	353 (19)	12.3 (2.2)	3.5 (0.3)	14.1 (2.8)	15.2 (3.0)
	Chitosan	105 (17)	7.1 (1.4)	3.8 (0.2)	20.7 (1.2)	22.1 (2.8)
	Bioactive glass	4125 (915)	114.5 (12.2)	2.8 (1.3)	3.5 (0.8)	4.8 (4.2)
20	PEA	692 (31)	22.3 (3.3)	3.2 (0.4)	7.2 (3.0)	8.5 (3.2)
	Chitosan	121 (28)	8.7 (2.2)	3.2 (0.4)	18.2 (3.4)	19.6 (4.7)
	Bioactive glass	- <sup>4)</sup>	-	-	-	-

1) Scale parameter for aspect ratio

2) Shape parameter for aspect ratio

3) Parentheses are standard deviation (SD).

4) Can not be obtained.

two systems. It might be due to more possibly existing higher hydrogen and chemical bonds between silanol and carboxyl or hydroxyl groups. IFSS of chitosan fiber/PLLA composite was higher than that of PEA/PLLA composite. It is considered because chitosan fiber has higher surface roughness that induced mechanical interlocking, compared to relatively smooth surface of PEA fiber. The decreasing rate of IFSS was the fastest in bioactive glass fiber/PLLA composite, whereas that of chitosan fiber/PLLA composite was the slowest. Hydrolytic resistance at the interface could not be strong because bioactive glass fiber contains many hydrophilic groups such as silanol group, SiOH on the surface.

Figure 10 shows SEM photographs of PEA, chitosan and bioactive glass fibers before and after hydrolysis. Initially chitosan fiber exhibits rougher surface compared to PEA and bioactive glass fibers. After 5 days, bioactive glass fiber exhibited rough surface and decreased diameter steeply, whereas diameter and surface roughness of chitosan fiber rarely changed until 10 days. Although the diameter of PEA fiber decreased slightly compared to the initial state, surface roughness did not change. It could be considered that total molecular weight decreased uniformly on the whole fiber

surface without of local microcracks.

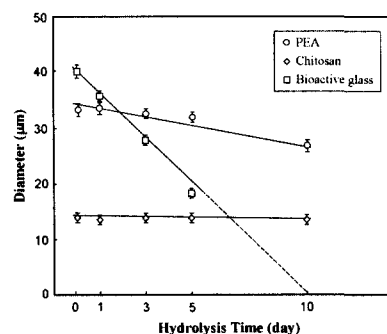


Fig. 8 Change of diameter for bioabsorbable fibers with hydrolysis time

Table 5 shows the change of Weibull distribution parameters, average fragments length and IFSS of bioabsorbable PEA, chitosan, and bioactive glass fibers/PLLA composites with hydrolysis time. Average fragment length of PEA fiber increased gradually and IFSS decreased with hydrolysis time, whereas after either 5 or 10 days IFSS increased slightly more than the initial state. It might be due to the increased degree of crystallinity as reported in previous



work [20]. At 15 days, IFSS began to decrease and at 20 days IFSS became about one half compared to the initial state. For chitosan fiber, IFSS did not change within the error range until 15 days, and it began to decrease slightly at 20 days. IFSS between bioactive glass fiber and PLLA matrix decreased rapidly unlike other two cases.

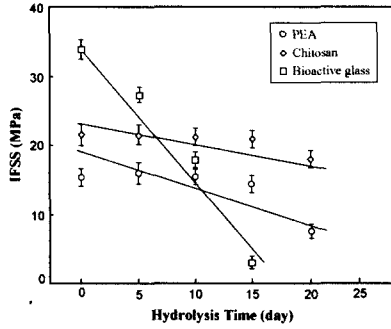


Fig. 9 Change of IFSS of bioabsorbable fiber/PLLA composites with hydrolysis time

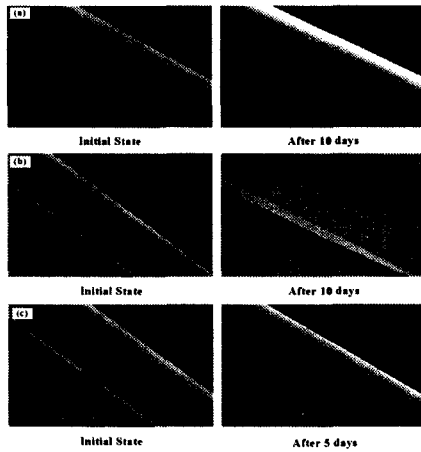


Fig. 10 Surface photographs of 3 bioabsorbable fibers in initial state and after degradation: (a) PEA, (b) chitosan, and (c) bioactive glass fiber

Figure 11 shows microfailure modes of bioabsorbable 3 fibers reinforced PLLA composites: (a) PEA; (b) chitosan; and (c) bioactive glass fiber. Decreased fragments length and different patterns of fiber breakage could be observed. In the initial state, PLLA matrix was transparent, whereas it began to be semi-transparent at 5 days because of the creating crystalline. Since tensile strength of bioactive glass fiber was

higher than other two fibers, stress-whitening distribution induced by bioactive glass fiber fracture was larger and clearer in the initial state. Stress whitening degree of chitosan fiber was smaller than those of PEA fiber. It might be because the failure of chitosan fiber occurred partially by microfibril fracture, whereas PEA fiber might result in monofilament failure accompanying with local plastic deformation. As hydrolysis went on, stress-whitening state for bioabsorbable 3 fibers decreased gradually, and the phenomena of the interfacial degradation began to appear. This degradation was the fastest comparatively in bioactive glass fiber having the rapid degradation rate.

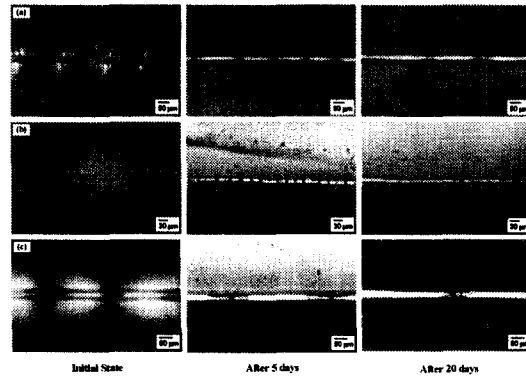


Fig. 11 Microfailure modes of 3 bioabsorbable fibers/PLLA composites with hydrolysis time: (a) PEA, (b) chitosan, and (c) bioactive glass fiber

### 3.3 AE Outcomes and Correlation with Microfailure Modes

The microfailure modes of fiber could be observed directly via an optical microscope, whereas AE signals for fiber fracture could be monitored using a piezoelectric transducer in the center of the SFC specimen. It was interested in detecting the microfailure signals of bioabsorbable fibers to correlate failure modes with hydrolysis.

Figure 12 shows the typical microfailure modes of PEA fiber. In the initial state, PEA fiber showed ductile microfailure mode such as diagonal fracture, whereas at 10 days vertical fracture appeared due to the increased brittleness of PEA fiber based on hydrolysis. The number of fragments increased with elapsing hydrolysis time. Figure 13 shows typical microfailure modes of bioactive glass fiber under (a)

tensile and (b) compressive tests. In tension brittle microfailure modes such as diamond cone-shaped vertical fracture appeared, whereas overlapped fiber slippage exhibited in compression.

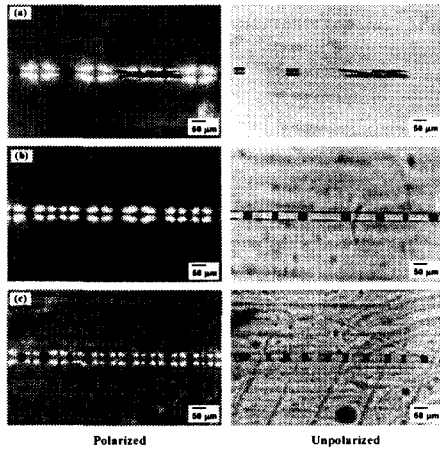


Fig. 12 Microfailure modes of PEA fiber with hydrolysis time in (a) the initial state, (b) after 5 days, and (c) after 10 days

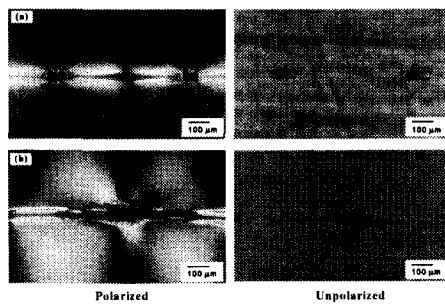


Fig. 13 Microfailure modes of bioactive glass fiber under (a) tensile and (b) compressive tests.

AE energy being calculated from the formula composed of signal amplitude and duration time, might be also related to fracture energy [21]. Figure 14 shows AE amplitude and AE energy of PEA fiber with measuring time. As hydrolysis time went on, AE amplitude and AE energy of PEA fiber decreased, and their distributions became narrower gradually. It may be due to the decreased fiber fracture energy and the change of microfailure modes based on hydrolysis reaction. The reason for initially broad distribution is because diagonal and vertical fiber failures may occur simultaneously, which

may have different fracture energies. On the other hand, with hydrolysis progressed, many vertical failure having weak and uniform fracture energies occurs due to enhanced fiber brittleness by degradation without diagonal failure. These results were consistent with microfailure modes by SFC test.

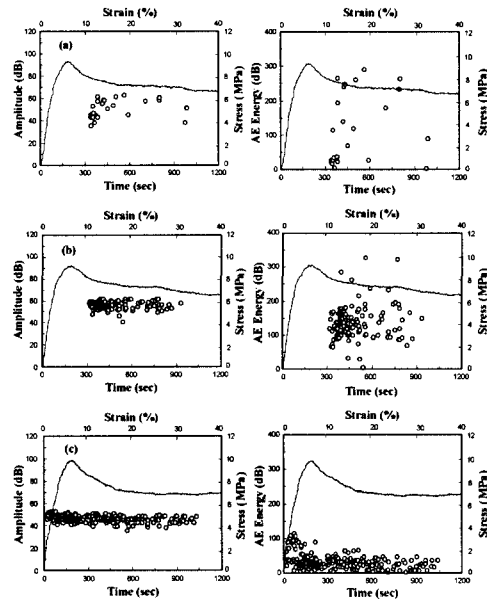


Fig. 14 AE amplitude and AE energy of PEA fiber with hydrolysis time: (a) the initial state, (b) after 5 days, and (c) after 10 days

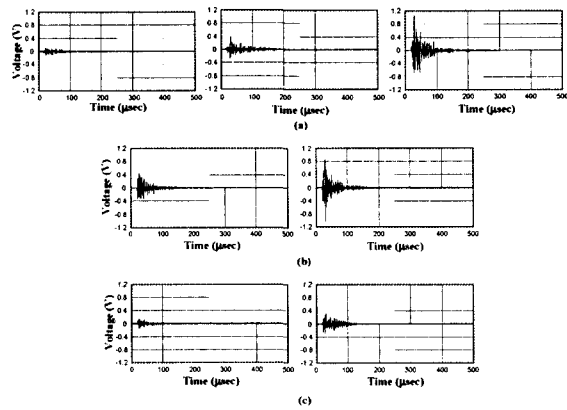


Fig. 15 AE waveforms of PEA fiber with hydrolysis time: (a) the initial state, (b) after 5 days, and (c) after 10 days

Figure 15 shows the AE waveforms for PEA fiber with

hydrolysis time. In the initial state, three kinds of waveform appeared, which could describe the relationship between AE amplitude distribution and microfailure modes. It is considered that AE amplitude distribution shows broad range from 35 to 65 dB as shown in Figure 14 (a). As hydrolysis time elapsed, the highest and intermediate AE waveforms were detected and then finally the lowest and intermediate waveforms appeared. It might be because of narrow AE amplitude distribution due to decreased fiber fracture energy as hydrolysis continued. AE amplitude and AE energy of chitosan fiber with hydration time at (a) the initial state and (b) after 10 days were shown in Figure 16. AE amplitude and AE energy were almost same, since mechanical properties of chitosan fiber did not change significantly within testing time range.

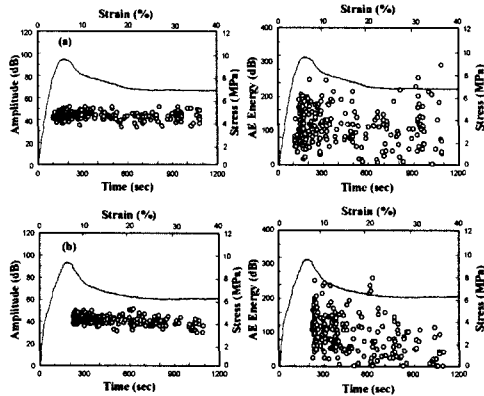


Fig. 16 AE amplitude and AE energy of chitosan fiber with hydrolysis time: (a) the initial state, and (b) after 10 days

Figure 17 shows AE results for bioactive glass fiber with stress-strain curves under tensile and compressive. For both the initial and after degradation cases, AE amplitude and AE energy in tensile failure were much higher than those of compressive test. It is probably because of the difference in fracture modes and energies between the axial compressive loading in tension and the transverse tensile loading in compression. Generally, fiber breaks occurred until around yielding point in tension. Beyond yielding point, AE events were not detected because of the absence of interlayer and matrix failures under tensile test as previous work [22] whereas in case of compression AE events occurred from the interlayer failure and matrix buckling just after yielding point.

AE amplitude and AE energy at the initial state were much higher than those of after degradation for both tension and compression.

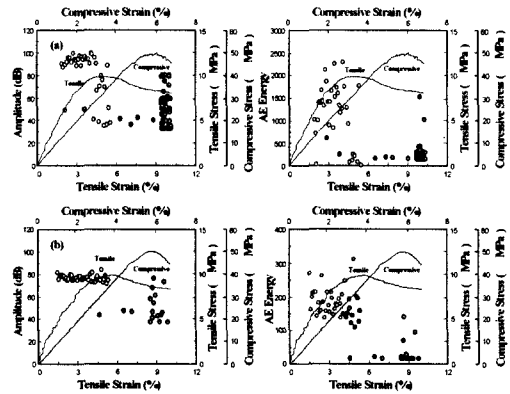


Fig. 17 AE amplitude and AE energy of bioactive glass fiber with hydrolysis time under tensile and compressive test: (a) the initial state, and (b) after 3 days

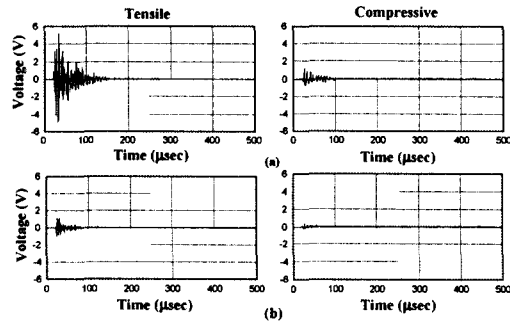


Fig. 18 AE waveforms of bioactive glass fiber with hydrolysis time under tensile and compressive test: (a) the initial state, and (b) after 3 days

Figure 18 shows AE waveforms of bioactive glass fiber under tensile and compressive loadings. Tensile fracture signals of bioactive glass fiber showed much higher than those of compressive test for both the initial state and after degradation as described above. Unlike polymeric PEA fiber, however, the primary and secondary bonding approach cannot be suitable for the isotropic glass fiber case. Only different failure mechanisms depending on loading conditions can explain this difference. AE waveforms in the initial state were much higher than those of after degradation for both tests. It might be due to the decreased fiber diameter and tensile strength significantly.

#### 4. CONCLUSIONS

Micromechanical tests combined with AE were investigated to obtain the interfacial properties and microfailure degradation mechanisms of bioabsorbable composites with hydrolysis time. As hydrolysis time went on, the mechanical properties bioactive glass fibers decreased steeply and those of PEA fiber decrease gradually, whereas chitosan fiber almost did not change. IFSS between bioactive glass fiber and PLLA was much higher than other two systems. The decreasing rate of IFSS was the fastest in bioactive glass fiber/PLLA composite, whereas that of chitosan fiber/PLLA composite was the slowest. Although the initial interfacial bonding of bioactive glass fiber composite was strong, the resistance on degradation with hydrolysis was rather poor. In the case of the stability of hydrolytic degradation can be enhanced, bioactive glass fiber/PLLA composite may be applied to bioabsorbable implant materials. PEA fiber showed ductile microfailure modes at the initial state, whereas brittle microfailure modes appeared with elapsing hydrolysis time. In addition, the distribution of AE amplitude was narrow and AE energy decreased gradually. It may be due to the deteriorated fiber fracture energy as well as the change of microfailure modes. AE amplitude and AE energy for bioactive glass fiber in tensile failure were much higher than those of compressive test. It might be because the difference in the fracture mechanisms between tensile and compressive fracture. AE parameters of bioactive glass fiber at the initial state were much higher than those of after degradation for both tests. Results of nondestructive AE were consistent with microfailure modes by fragmentation test and optical observation.

#### ACKNOWLEDGMENT

This work was financially supported by Research Center for Aircraft Parts Technology (ReCAPT), GNU.

#### REFERENCES

- 1) Böstman, O. M., Makela, E. A., Törmälä, P. and Rokkanen P., *J. Bone Joint Surg.*, Vol. 71B, 1989, pp. 706-707.
- 2) Böstman, O. M., *Clinic Ortho.*, Vol. 329, 1996, pp. 233-239.
- 3) Sinibaldik, K., Rosen, H., Lin, S. K. and De Angelis, M., *Clinic Ortho. Rel. Res.*, Vol. 118, 1976, pp. 257-266.
- 4) Thomson, R. C., Yaszemski, M. J., Powers, J. M. and Mikos, A. G., *Biomater.*, Vol. 19, 1998, pp. 1935-1943.
- 5) Slivka, M. A., Chu, C. C. and Adisaputro, I. A., *J. Biomed. Mater. Res.*, Vol. 36, 1997, pp. 469-477.
- 6) Andriano, K. P., Wenger, K. H., Daniels, A. U. and Heller, J., *J. Biomed. Mater. Res.*, Vol. 48, 1999, pp. 528-533.
- 7) Nijenhuis, A. J., Colstee, E., Grijpma, D. W. and Pennings A. J., *Polym.*, Vol. 37, 1996, pp. 5849-5857.
- 8) Park, J. M. and Subramanian, R.V., *J. Adhes. Sci. Technol.*, Vol. 5, 1991, pp. 459-477.
- 9) Kelly, A. and Tyson, W. R., *J. Mech. Phys. Sol.*, Vol.13, 1965, pp. 329-350.
- 10) Favre, J. P. and Jacques, D., *J. Mater. Sci.*, Vol. 25, 1990, pp. 1373-1380.
- 11) Lee, S. I., Park, J. M., Shin, D. W. and Yoon, D. J., *Polym. Compos.*, Vol. 20, 1999, pp. 19-28.
- 12) Ageorges, C., Friedrich, K., Schüller, T. and Lauke, B., *Compo. Part A*, Vol. 30, 1999, pp. 1423-1434.
- 13) Wood, J. R. and Marom, G., *Appl. Compos. Mater.*, Vol. 4, 1997, pp. 117-124.
- 14) Park, J. M., Chong, E. M., Yoon, D. J. and Lee, J. H., *Polym. Compos.*, Vol. 19, 1998, pp. 747-757.
- 15) Ma, B. T., Schadler, L. S., Laird, C. and Figueroa, J. C., *Polym. Compos.*, Vol. 11, 1990, pp. 211-216.
- 16) Drzal, L. T., Rich, M. J., Koeng, M. F. and Lloyd, P. F., *J. Adhes.*, Vol. 16, 1983, pp. 133-152.
- 17) Wu, H. F. and Netravali, A. N., *J. Mater. Sci.*, Vol. 33, 1992, pp. 3318-3324.
- 18) Park, J. M., Shin, W. G. and Yoon, D. J., *Compos. Sci. Technol.*, Vol. 59, 1999, pp. 355-370.
- 19) Chu, C. C., In: Wise, D. L. Editors. *Encyclopedic handbook of biomaterials and bioengineering*, New York, Marcel Dekker, 1995.
- 20) Park, J. M. and Kim, D. S., *Polym. Compos.*, Vol. 21, 2000, pp. 789-797.
- 21) Kline, R., In: Matthews, J. R. Editors, *Acoustic Emission*, New York, Gordon Breach, 1983.
- 22) Park, J. M., Kim, Y. M., Kim, K. W. and Yoon, D. J., *J. Col. Interf. Sci.*, Vol. 231, 2000, pp. 114-128.